Experimental Investigation of a Novel Two-stage Heat Recovery Heat Pump System Employing the Vapor Injection Compressor at Cold Ambience and High Water Temperature Conditions

Yunhai Li [a, **], Zhaomeng Li [a, **], Yi Fan [b], Cheng Zeng [a], Yu Cui [a], Xudong Zhao [a, *], Jing Li [a, *], Ying Chen [c], Jianyong Chen [c], Chao Shen [d]

[a] Centre for Sustainable Energy Technologies, University of Hull, Hull, HU6 7RX, UK
[b] College of Energy and Mechanical Engineering, Shanghai University of Electric Power, Shanghai 201306, China
[c] School of Material and Energy, Guangdong University of Technology, Guangzhou 510006, China
[d] School of Architecture, Harbin Institute of Technology, Harbin 150090, China
* Corresponding author. Tel.: +44-01482466684 (X. Zhao), +44-01482463611 (J. Li).
E-mail addresses: Xudong.zhao@hull.ac.uk (X. Zhao), Jing.li@hull.ac.uk (J. Li).
** These authors contributed equally to this work

Abstract:
Heat pumps (HPs) are energy-efficient space heating devices that are key to global carbon reduction and carbon neutrality. However, current commercial HPs have performance issues in cold climates where space heating is needed most, including low COP and high energy consumption of defrosting. Aiming to tackle these issues, a novel two-stage heat recovery heat pump (THRHP) is therefore developed to enable heat recovery from exhaust air for improving COP and preventing dramatic energy use during winter defrosting. The performance of THRHP was optimized in the laboratory by investigating its expansion valve opening and exhaust air fans situation. Finally, the experiment results showed the prototype provided a heating capacity of 32.3 kW, generating 4 m^3/h hot water of 55 °C with COP of 2.57 at outdoor temperature of 0 °C, achieving 20.1% higher COP than the commercial HPs, while the efficient and quick defrosting process only consumed 0.46 kW and 4 minutes under outdoor temperature on -6 °C. The results gave more insights into the characteristics of THRHP and obtained the optimal control strategies of THRHP for better performance, thus promoting the wide deployment of HPs and achieving the ambitious carbon-neutrality targets.

Keywords: Heat pump, exhaust air, heat recovery, defrosting, performance optimization.

Nomenclature

Symbols		eco	economizer
Q	heat capacity (kW)	ME	medium-pressure evaporator
W	power consumption (kW)	LE	low-pressure evaporator
h	specific enthalpy (kJ/kg)	L	low-pressure compression
$\dot{m}$	mass flow rate (kg/s)	H	high-pressure compression
c	specific heat capacity (kJ/kg/K)	r	refrigerant
U	uncertainty (%)	w	water
P	pressure (MPa)	a	air
HR	high-pressure compression ratio	in	inlet
LR	low-pressure compression ratio	out	outlet
TR	Total compression ratio	inj	vapor injection
H	compression head (kW)	i	indoor
Subscripts		o	outdoor
com	compressor	**Abbreviations**	
con	condenser	*COP*	coefficient of performance

1 Introduction

1.1 The background and motivation

The global CO_2 emission has increased by around 1.3% per annum over the past five years, according to International Renewable Energy Agency (IRENA) [1]. This is caused by significant fossil fuel energy use. Especially the heating and hot water productions of buildings take up around 48% of the world's total energy use, of which 89% is from non-renewable energy, leading to approximately 40% of global CO_2 emission [2]. Therefore, utilizing low-carbon heating techniques is critical to decarbonizing buildings.

Many countries have committed to employing low-carbon heating techniques in buildings. According to International Energy Agency (IEA), heat pumps could meet 90% of global heating needs and nearly 180 million heat pumps have been installed for heating in 2020, taking up by North America 40.1 million units, Europe 21.8 million units, China 57.7 million units, and other countries of over 50 million units [3]. By 2050, according to IRENA, the global heat pump installations will increase to 253 million [1]. The enormous heat pump market in buildings is supported by high-level guidelines and incentives. For instance, through the UK's Heat and Buildings Strategy in 2021, households will benefit from a grant of £5,000 to install low-carbon heating systems like heat pumps and the UK government aims to phase out natural gas boiler installations from 2035 [4]. In the east, China is taking a major energy transition from fossil fuel to low-carbon energy, aiming to peak the carbon emission level before 2030 and reach carbon neutrality by 2060. China has issued a series of policies along with subsidies to promote heat pumps such as the Guidance on Promoting Electric Power substitution and Clean Energy Heating Plan for Winter in Northern China [5].

1.2 The challenges and status of air source heat pumps

For technology, air source heat pumps (ASHPs), which can effectively absorb heat from the ambient with low electricity consumption have been dominating global heat pump sales for their ease of installation and relatively low installation costs. While, despite the increasing market share of air source heat pumps and the government support of utilization, the inherent performance challenges remain, especially for the ASHPs operating in the low outdoor temperature. The main performance challenges are listed:

(1) The heating capacity decreases in cold climates since the air source heat pumps are based on the vapor compression cycle where the evaporation temperature as well as the refrigerant flow rate decreases as the outdoor temperature drops.
(2) An additional heating element is used to meet the increasing heating demand of the cold climates, leading to a low energy performance across the cold season.
(3) The power consumption increases with water temperature while cold climates require higher water temperature. The high water temperature also leads to high

compressor discharge temperature, causing damage to the heat pump's lifetime.

(4) As the outdoor unit extracts heat from the ambient, frost forms on the outdoor heat exchanger, increasing the heat transfer resistance and airflow resistance, which can consume more energy for defrosting.

(5) For indoor spaces requiring ventilation, the indoor heat is lost during the ventilation process without appropriate heat recovery equipment, thereby increasing the space heat load and adding pressure to the heat pumps.

To tackle the listed challenges, the literature has seen many studies on components or process innovations. The components innovations include but are not limited to the use of ejectors [6, 7] and trials of new refrigerants [8, 9], or regulating compressor’s working conditions by extracting the excessive heat [10, 11], etc. New refrigerants especially a blend of refrigerants can increase the heating performance for the thermodynamic potential and tackle the global warming effect caused by the use of hydrofluorocarbons [12].

In addition to the component innovations, many numerical or experimental studies have been published in process innovations for improving the cold climate heating performance, examples like multiple-stage compression, vapor injection, and exhaust heat recovery. Among them, the multiple-stage compression ASHPs can effectively increase the system efficiency by reducing the compression ratio of each stage in cold climates. Bertsch et al. [13] proposed several two-stage compression ASHP cycles for cold climates, whose test results indicate the prototype has COP of 2.1 at -30 ºC outdoor temperature. The application research of the prototype further proved that this novel ASHP has 19% energy saving compared to the gas furnace system [14]. However, Bertsch’s studies stress the high cost of the system complexity and call for improvements in process controls.

To simplify the complexity and cost of the multiple-stage compression ASHPs, The concept of vapor injection ASHP using an economizer or flash tank was proposed in the 1970s [15], which is another promising approach to increase the heating capacity and reduce the compressor discharge temperature in cold climates. Shen et al. [16] experimentally investigated a tandem vapor injection compression heat pump, which performed stable and good heating performance when outdoor temperature decreases from 8 ºC to -34 ºC. Lu et al [17] designed a vapor-injected photovoltaic-thermal heat pump and experimentally compared it with the normal photovoltaic-thermal heat pump, which confirmed that the vapor-injected system has 30% and 10% improvement in heating capacity and COP, respectively.

Heat recovery heat pump is another engaging process upgrade that many researchers have been working on which extracts a proportion of the thermal energy from the indoor exhaust air [18-20]. Gustafsson et al. [21] numerically evaluated the energy performance of three heat recovery heat pump configurations, including heat recovery in air-to-air heat pumps and air-to-water heat pumps. The evaluations showed that the heat recovery heat pumps are favorable for cold climates by either increasing the heat source temperature or recovering the indoor thermal energy as part of the heat output. Recent studies are mainly focused on residential applications. Although they reported a higher COP as part of the energy performance index, the heating capacity was relatively small because of the limited heat energy from a single heat source of the exhaust air [22].

Apart from the technological advancement for energy performance, frosting is another key challenge for the ASHPs operating in cold climates, which will lead to a relatively high defrosting energy consumption [23]. Many studies have been reported around the defrosting or low energy frost retarding concepts, where Song et al. [24] presented a comprehensive review of the techniques including changing the ambient air parameters like preheating the inlet air, frost vibration techniques, external coil optimizations, and heat pump process optimizations. The aim of the frost-related heat pump studies is low defrosting energy input for defrosting or frost prevention along with minimizing the defrosting impact on the indoor heat supply.

1.3 The innovations and contributions of the study

Tackling the performance challenges of ASHPs in cold climates requires a combination of innovations, and more importantly takes up first-hand learnings from a real-life project to obtain the primary performance data for further improvements in applications and control strategies. To address the research gap and add value to the ASHP literature from a real-life project, this paper manufactures a novel two-stage heat recovery heat pump (THRHP) for real-life demonstration, whose performance is investigated and compared with the heat pumps on the market. The presented THRHP prototype integrates a series of innovations to address the current ASHP performance challenges. For effective heat recovery and increasing heating capacity in cold climates, the THRHP extracts heat from the indoor exhaust air and the outdoor environment using two-stage evaporation. Further, it is equipped with a vapor injection compressor to boost the compressor performance and utilizes exhaust air to prevent frost formation in cold climates along with significantly reducing the defrosting power consumption and defrosting time.

In this study, the prototype is optimized and tested over a wide range of outdoor temperatures and high water outlet temperature conditions. The heating performance results are analyzed under different working conditions, and with and without exhaust air heat recovery, gaining deep insights into the performance characteristics of THRHP, and finally, the optimum performance of THRHP is compared with the commercial heat pumps. The studies will reveal the operational characteristics and the application advantages of THRHP in low-carbon heating, thus providing constructive guidance for the practical deployment and optimal control of the THRHP to achieve a renewable heating future.

2 The Descriptions of THRHP

2.1 The principle of the THRHP

Figure 1 shows the schematic flow diagram of the THRHP including the refrigerant flow and airflow directions. The major components are the medium-pressure evaporator (ME), low-pressure evaporator (LE), economizer, expansion valves of the ME, LE and economizer, vapor injection compressor, plate-type condenser, and air circulation fans. To maximize the heat recovery from exhaust air and reduce the system's power consumption, the refrigerant ($\dot{m}_{\mathrm{r}}$) is divided into three streams after it is subcooled by the condenser with water. The first refrigerant steam ($\dot{m}_{\mathrm{r},1}$) goes into the economizer for further subcooling before being throttled at the expansion valve of low-pressure evaporator (EVL) and evaporated in the LE. The second stream ($\dot{m}_{\mathrm{r},2}$) is throttled by the expansion valve of economizer (EVE) and evaporated in the economizer. The third stream ($\dot{m}_{\mathrm{r},3}$) is throttled by the expansion valve of medium-pressure evaporator (EVM) and evaporated in the ME. Following the economizer and two evaporators, the refrigerant is diverted into the compressor where the first stream travels to the compressor inlet, and the other two streams flow into the vapor injection inlet. Respecting the airflow, the indoor exhaust air goes to the ME, meanwhile, the outdoor air is extracted into the system to mix with the exhaust air from the ME before flowing across the LE. The fresh air will flow into the room as the indoor air was discharged, fulfilling the ventilation requirement of the building. According to the working principle, Figure 2 depicts the pressure-enthalpy diagram of the refrigerant circuit of THRHP (see the black lines), and Table 1 lists the corresponding energy and mass conservation equations.

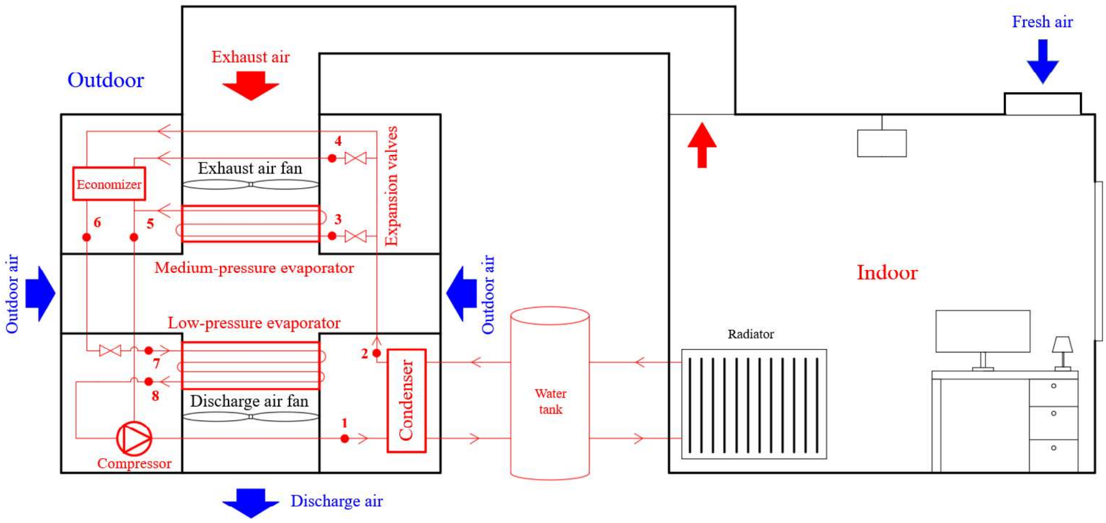

Figure 1. The system diagram of THRHP

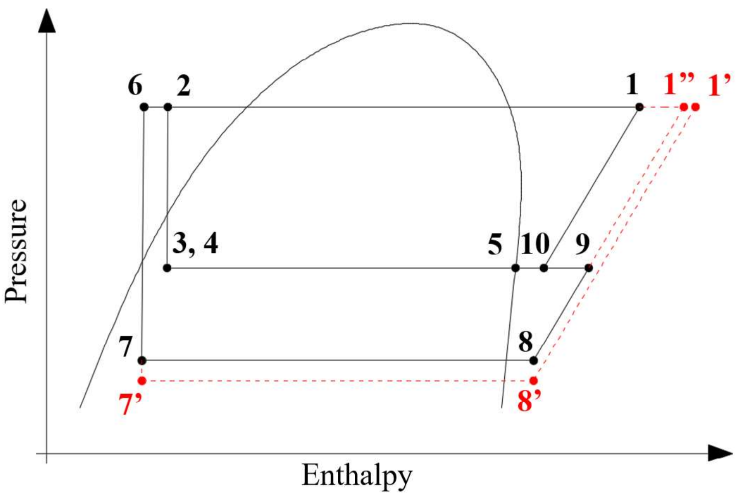

Figure 2. The pressure-enthalpy diagram of THRHP

Table 1. Energy and mass conservation equations of THRHP

Working procedures	Equations
Condenser heat transfer (1-2)	$Q_{con}=\dot{m}_r(h_1-h_2)$
Economizer heat transfer (2-6, 3-5)	$Q_{eco}=\dot{m}_{r,1}(h_2-h_6)=\dot{m}_{r,2}(h_3-h_5)$
ME heat transfer (3-4)	$Q_{ME}=\dot{m}_{r,3}(h_4-h_5)$
LE heat transfer (6-7)	$Q_{LE}=\dot{m}_{r,1}(h_8-h_7)$
Low-pressure compression (7-8)	$W_L=\dot{m}_{r,1}(h_9-h_8)$
Mixing chamber (4, 8-9)	$h_{10}=\frac{(\dot{m}_{r,2}+\dot{m}_{r,3})h_5+\dot{m}_{r,1}h_9}{\dot{m}_r}$
High-pressure compression (9-1)	$W_H=\dot{m}_r(h_1-h_{10})$
Energy conservation	$Q_{con}=Q_{eco}+Q_{LE}+Q_{ME}+W_L+W_H$
Mass conservation	$\dot{m}_r=\dot{m}_{r,1}+\dot{m}_{r,2}+\dot{m}_{r,3}$
Heating capacity	$Q=Q_{con}$
Power consumption	$W=W_L+W_H$
Coefficient of performance (*COP*)	$COP=\frac{Q}{W}$

Compared to a conventional ASHP following 1’-6-7’-8’ in Figure 2 the THRHP presents the following outstanding characteristics:

(1) The two-stage vapor injection compression decreases the discharge temperature as well as the compressor enthalpy from 1’ to 1 by injecting saturated refrigerant 5 into the superheated refrigerant 9. Also, the compression process is divided into two stages with smaller compression ratios which can improve the compression

efficiency. Therefore, the power consumption of THRHP decreases when compared to the conventional ASHP. In addition, due to the vapor injection refrigerant, the total refrigerant mass flow rate in point 1 is larger than that of the conventional ASHP, benefiting the higher heating capacity of THRHP.

(2) The two-stage exhaust air heat recovery improves the evaporation process, leading to various advantages. Firstly, the novel design of ME, recovering waste heat from the exhaust air further enlarges the injection refrigerant mass flow rate of point 5 and thus increases the total refrigerant mass flow rate of point 1 as well as the heating capacity of THRHP. After the exhaust air mixes with the outdoor air and flows through the LE, the evaporating pressure of LE rises from 7' to 7 because of the higher mixing air temperature, which leads to a smaller pressure ratio in process of 8 to 9 as well as further decreasing power consumption of THRHP.

(3) The exhaust air heat recovery increases the evaporating temperature, which minimizes frosting risk and thus defrosting energy consumption. Additionally, benefiting from the larger temperature difference between the exhaust air and the frost on LE, a defrosting process by exhaust air fans is energy efficient without the compressor, i.e., low defrosting power consumption and short defrosting time.

2.2 The design of the THRHP prototype

Figure 3 shows the structure of the manufactured THRHP prototype, whose key components are a vapor injection compressor, a plate condenser, an economizer, five air fans, one ME, two LEs and three electronic expansion valves (see Table 2). Notably, there are 2 exhaust air fans on the top of THRHP to extract the exhaust air and 3 discharge air fans on the bottom of THRHP to divert the air out of the system. During a heat supply mode, the fans extract both indoor and outdoor air for heat exchange in ME and LE. During a defrosting operation, the exhaust air fans are turned on while the discharge air fans are turned off. Switching off the discharge air fans mechanically drops the one-way louver at the outdoor air intake vents and shuts the outdoor air entrance, at that time, the warm exhaust air can defrost swiftly by consuming little power from exhaust air fans.

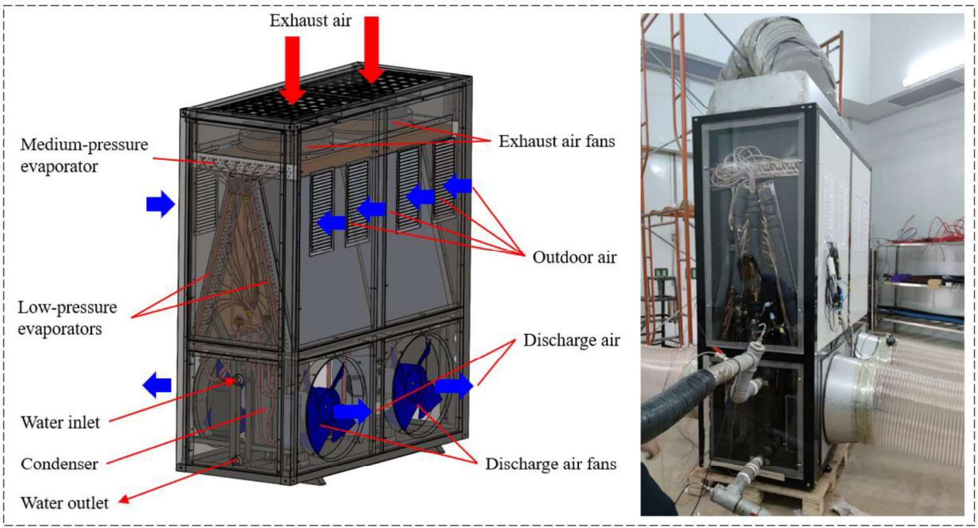

Figure 3. The structure of the THRHP prototype

Table 2. Components details of the THRHP prototype

Components	Parameters	Specifications
Compressor	Model	Emerson ZW258HSP-TFP-522
	Type & amount	Hermetic scroll * 1
	Displacement (cm^3/r)	124
	Refrigerant	R410a
Condenser	Model	SWEP P80Hx120/1P-SC-M
	Type & amount	Plate type heat exchanger * 1
	Size (length * width * height (mm))	191 * 273 * 526
Economizer	Model	Haolei HL20-60D
	Type & amount	Plate type heat exchanger * 1
	Size (length * width * height (mm))	76 * 143 * 310
Medium-pressure evaporator	Model	FIVESTAR DKRS13(13x).03
	Type & amount	Fin-and-tube heat exchanger * 1
	Size (length * width * height (mm))	1650 * 98 * 602
Low-pressure evaporator	Model	FIVESTAR DKRS-13(13X).02.01
	Type & amount	Fin-and-tube heat exchanger * 2
	Size (length * width * height (mm))	1650 * 100 * 1000
Expansion valve of Economizer	Model	Sanhua DPF(Q)2.4C-11-RK
	Diameter of valve port (mm)	2.4
	Maximum working pressure (MPa)	4.2
Expansion valve of low-pressure evaporator	Model	Sanhua DPF(Q)3.0C-08
	Diameter of valve port (mm)	3.0
	Maximum working pressure (MPa)	4.2
Expansion valve of medium-pressure evaporator	Model	Sanhua FDF4A10
	Diameter of valve port (mm)	4.0
	Maximum working pressure (MPa)	4.2
Exhaust air fan	Model	Songgang YDK-90-6
	Type & amount	Fixed frequency fan * 2
	Nominal speed	750 ± 30
	Size (diameter * height (mm))	490 * 125
Discharge air fan	Model	Songgang YDK-250-6

Type & amount	Fixed frequency fan ∗ 3
Nominal speed (r/min)	880 ± 30
Size (diameter ∗ height (mm))	556 ∗ 167

2.3 The performance test platform and procedure

The THRHP was tested thoroughly in the environmental chamber (see Figure 4), which enabled the adjustment to the air temperature, air humidity, water temperature and flow rate. First of all, the refrigerant charge of the THRHP was preferentially optimized under fixed working conditions, i.e., the outdoor temperature of -12 ºC, and water outlet temperature of 55 ºC with a water flow rate of 4 m^3/h. The optimum refrigerant charge of THRHP was set to 13 kg at last. Thereafter, during the performance tests, the environmental chamber maintained the THRHP outdoor temperature, water outlet temperature and water flow rate at the setpoint while the EVL opening was adjusted carefully to achieve the best COP of THRHP. The tested outdoor temperature ranged from -12 ºC to 18 ºC with an increment of 6 ºC, and the water outlet temperature reached three high temperatures, namely 41 ºC, 48 ºC, and 55 ºC with a fixed water flow rate of 4 m^3/h, which covered a wide range of heat pump working conditions representing cold and mild regions. Subsequently, the impact of exhaust air heat recovery was investigated by removing the THRHP exhaust air cover and air duct and closing the exhaust air fans. The prototype's COP without the exhaust air was also optimized by adjusting the EVL opening under the same test conditions before comparison. The experimental conditions are stated carefully in Table 3. During the experiments, the air and refrigerant temperatures of THRHP are measured by thermocouples. The refrigerant pressures are measured by pressure transducers. The space temperatures and water temperatures are measured by Pt-1000 platinum resistors, and the power consumption of THRHP is recorded by the power meter, whose accuracies are listed in Table 4.

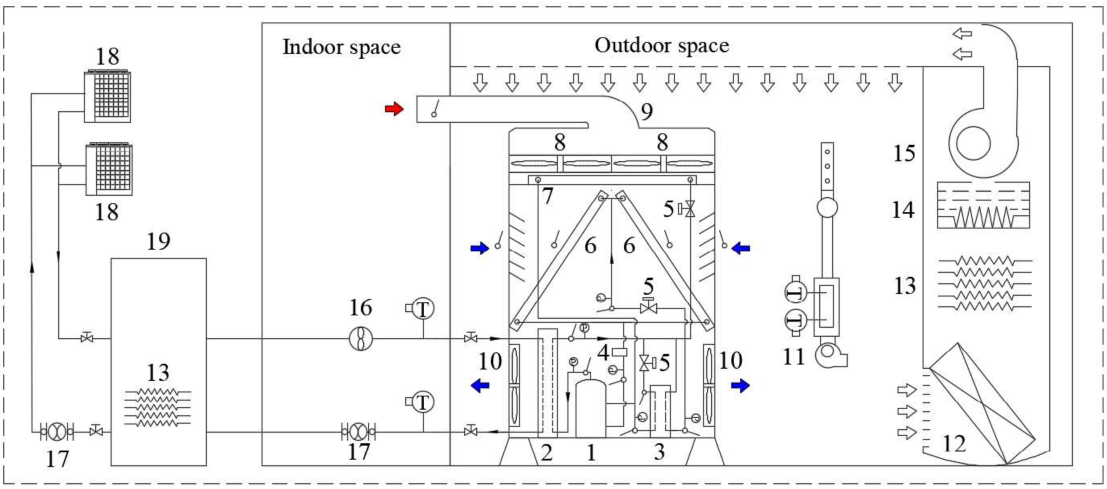

1.Compressor, 2.Plate condenser, 3.Economizer 4.Storage tank, 5.Electronic expansion valve, 6.Low-pressure evaporator, 7.Medimum-pressure evaporator, 8. Exhaust air fan, 9.Exhaust air cover and duct, 10. Discharge air fan, 11.Example collector, 12.Cooler, 13.Heater, 14.Humidifier, 15.Air blower, 16.Electromagnetic flowmeter, 17.Water pump, 18.Water chiller, 19.Water tank, Ⓣ PT-1000, Thermal couple, Ⓟ Pressure transducer

Figure 4. The THRHP experiment setup and environmental chamber

Table 3. Experimental conditions of the THRHP

Refrigerant charge (kg)	Water flow rate (m^3/h)	Exhaust air fans (On/Off)	Outdoor air temperature (°C)	Water outlet temperature (°C)
13	4	On	-12	41
				48
				55
			-6	41
				48
				55
			0	41
				48
				55
			6	41
				48
				55
			12	41
				48
				55
			18	41
				48
				55
		Off	-12	41
			-12	55
			18	55

Table 4. The accuracy of experimental sensors

Parameters	Measurement	Uncertainty
Temperatures of refrigerant side (T_r, °C)	Thermocouple	± 0.5 °C
Temperatures of air side (T_a, °C)	Pt-1000	± 0.15 °C
Temperatures of water side (T_w, °C)	Pt-1000	± 0.15 °C
Pressure (P_r, MPa)	Pressure transducer	± 0.5 %
Water flow rate ($\dot{m}_w$, m^3/h)	Electromagnetic flowmeter	± 0.5 %
Power consumption (W, kW)	Power meter	± 0.2 %

2.4 The key performance indicators

The key performance indicators of THRHP are the heating capacity, power consumption, and COP, supplemented by pressure ratios and refrigerant mass flow rate, which are given as follows.

The heating capacity (Q) of THRHP can be calculated by:

$$Q = c\dot{m}_{\mathrm{w}}(T_{\mathrm{w,out}} - T_{\mathrm{w,in}}) \quad (1)$$

where c is the specific heat capacity of water; $\dot{m}_{\mathrm{w}}$ is the water mass flow rate; $T_{w,out}$ and $T_{w,in}$ is the water outlet and inlet temperature, respectively.

The power consumption (W) of THRHP is measured by a power meter, and thus the COP of THRHP is evaluated by:

$$COP = \frac{Q}{W} \tag{2}$$

The pressure ratios of vapor injection compressor are expressed as:

$$LR = \frac{P_{\mathrm{r,\,inj,\,com}}}{P_{\mathrm{r,\,in,\,com}}} \tag{3}$$

$$HR = \frac{P_{\mathrm{r,\,out,\,com}}}{P_{\mathrm{r,\,inj,\,com}}} \tag{4}$$

$$TR = \frac{P_{\mathrm{r,\,out,\,com}}}{P_{\mathrm{r,\,in,\,com}}} \tag{5}$$

where LR, HR, and TR are low-pressure compression ratio, high-pressure compression ratio, and total pressure ratio, respectively; $P_{\mathrm{r,out,com}}$, $P_{\mathrm{r,in,com}}$ and $P_{\mathrm{r,in,inj}}$ is the refrigerant pressure of compressor outlet, compressor inlet and vapor injection inlet.

The total refrigerant mass flow rate is evaluated by:

$$\dot{m}_{\mathrm{r}} = \frac{Q}{h_{\mathrm{r,\,in,\,con}} - h_{\mathrm{r,\,out,\,con}}} \tag{6}$$

where $\dot{m}_{\mathrm{r}}$ is the total refrigerant mass flow rate; $h_{\mathrm{r,\,in,\,con}}$ and $h_{\mathrm{r,\,out,\,co}n}$ the refrigerant enthalpy of condenser inlet and outlet, respectively.

2.5 Uncertainty analysis

The uncertainties of the calculated data are accumulated from the uncertainties of the sensors, which are evaluated by the equations (7) and (8) [25]:

$$y = f\left(x_1, x_2, x_3, \cdots\cdots, x_{\mathrm{n}}\right) \tag{7}$$

$$U_y = \left[\left(\frac{\partial y}{\partial x_1} U_{x_1}\right)^2 + \left(\frac{\partial y}{\partial x_2} U_{x_2}\right)^2 + \left(\frac{\partial y}{\partial x_3} U_{x_3}\right)^2 \cdots\cdots + \left(\frac{\partial y}{\partial x_{\mathrm{n}}} U_{x_{\mathrm{n}}}\right)^2\right]^{0.5} \tag{8}$$

According to equation (8), the uncertainties of calculated data are listed in Table 5.

Table 5. Uncertainties of calculated data

Parameters	Uncertainty
Heating capacity (Q, kW)	± 5.58 %
Coefficient of Performance (COP)	± 0.59 %
Refrigerant mass flow rate ($\dot{m}_{\mathrm{r}}$, g/s)	± 4.56%
low-pressure compression ratio (LR)	± 3.35%
high-pressure compression ratio (HR)	± 3.69%

3 Results and discussions

This section presents and discusses the THRHP performance, including its heating capacity, power consumption, and COP. These performance indicators are closely linked to the outdoor temperature, water outlet temperature, EVL opening and exhaust air situation. On the basis of experiment results, the performance characteristics of THRHP are discussed to analyze the impact of EVL opening and exhaust air situations under different working conditions. Thereafter, detailed comparisons between the developed THRHP and commercial heat pumps are carried out at last.

3.1 Impact of working conditions on the THRHP performance

The performance characteristics of THRHP, including heating capacity, power consumption and COP, with outdoor/water outlet temperature are discussed first, followed by analyzation of the optimum opening of EVL.

3.1.1 The impact on the heating capacity of THRHP

Figure 5 illustrates the THRHP's heating capacity (HC) under the outdoor air temperature varying from -12 ºC to 18 ºC and the water outlet temperature varying from 41 ºC to 55 ºC. For simplicity, the descriptions of the test conditions are hereafter described in the order of outdoor temperature/water discharge temperature, e.g., 18 ºC/55 ºC. The 3D colour surface is the integrated effect of outdoor temperature and water outlet temperature on heating capacity (as shown in the black spots), whose X-Z projection (as shown in the red spots) further clears the characteristics of HC in relation to the outdoor temperature under the water outlet temperature of 41 ºC, 48 ºC, and 55 ºC, and the Y-Z projection (as shown in the blue spots) deeply illustrates the characteristics of HC in relation to water outlet temperature under the outdoor temperature of -12 ºC, -6 ºC, 0 ºC, 6 ºC, 12 ºC, 18 ºC.

Regarding the impact of the increasing outdoor temperature (see the X-Z projection of Figure 5), the increases in heating capacity result from a series of parameter interactions, including the refrigerant pressure, temperature, and mass flow rate of the THRHP. Starting from the refrigerant pressure, as shown in Figure 6, when outdoor temperature increases from -12 ºC to 18 ºC under a constant water outlet temperature, the compressor outlet pressure keeps constant, which means that the condensing heat transfer temperature difference is stable. However, the compressor inlet pressure raises by around 110%, while the vapor injection pressure raises by 79.5%, 43.6% and 22.6% at water outlet temperatures of 41 ºC, 48 ºC and 55 ºC, respectively, so as to the corresponding increases in the refrigerant density. In addition, as results of Figure 7 (a) and (c), the HR, LR and TR of the compressor decrease respectively by 17.2% to 42.6%, 13.8% to 42.8% and 50.5% to 55.2% with the outdoor temperature, which will lead to better volumetric efficiency, and thus increase the refrigerant mass flow rate of compressor. As results shown in Figure 8 (a), under the fixed compressor cylinder volume and the fixed rotation speed conditions, the total refrigerant mass flow rate in the condenser increases by 100.3%, 103.4% and 81.2% at water outlet temperatures of

41 ºC, 48 ºC and 55 ºC, respectively. And thus, the increasing total refrigerant mass flow rate boosts the condenser heat transfer coefficient as well as lifting the THRHP's heating capacity by 67.8%, 53.1% and 43.8% at water outlet temperatures of 41 ºC, 48 ºC and 55 ºC, respectively. It is noted that the increase of heating capacity is relatively larger in low water outlet temperatures. This is due to the decreases of the HR being significantly larger in low water outlet temperatures, leading to larger increases in the vapor injection refrigerant mass flow rate, so as to the total refrigerant mass flow rate and heating capacity.

Regarding the impact of water outlet temperature increasing from 41 ºC to 55 ºC (see the Y-Z projection of Figure 5), a higher water outlet temperature increases the THRHP's heating capacity by 17.5%, 18.3%, 13.7%, 9.1%, 2.8% and 0.6% at outdoor temperatures of -12 ºC, -6 ºC, 0 ºC, 6 ºC, 12 ºC and 18 ºC, respectively. Notably, the increase of THRHP's heating capacity with outdoor temperature is relatively sharp at low outdoor temperatures. From Figure 6 (b), under low outdoor temperatures, e.g., -12 ºC (see the black lines), the vapor injection inlet pressure increases by 88.7% as water outlet temperature increases from 41 ºC to 55 ºC, while compressor inlet pressure keeps constant. From Figure 7 (b) and (d), the HR decreases by 26.4%, while the TR of the compressor increases by 35.4%. As a result, the refrigerant mass flow rate of vapor injection inlet is significantly increased due to the increase in the vapor injection pressure and the decrease in the HR, while that of the compressor inlet is decreased because of the constant compressor inlet pressure and the increasing TR. Eventually, as shown in Figure 8 (b), the total refrigerant mass flow rate increases because of the significant increase in the vapor injection refrigerant mass flow rate, which benefits the increase of heating capacity at low outdoor temperatures at last. However, under high outdoor temperatures, e.g., 18 ºC, the increase of vapor injection inlet pressure (28.9%) and the decrease of the HR (5.7%) are narrowed, leading to small increases in the vapor injection mass flow rate. Eventually, the changes in total refrigerant mass flow rate are limited and thus leads to small changes in the heating capacity at high outdoor temperature.

Finally, from the 3D colour surface of heating capacity in Figure 5, the heating capacity of THRHP drops sharply in the direction of low outdoor temperature and low water outlet temperature, whose maximum and minimum are 39.1 kW at 18 ºC /55 ºC and 23.2 kW at -12 ºC /41 ºC, respectively. The THRHP can keep 59.3% of the maximum heating capacity in the worst conditions, which shows good stability. Further, in the conditions of cold weather, the heating capacity can be effectively increased by rising water outlet temperature, and thus better fulfil the high heating demand of buildings in cold weather days.

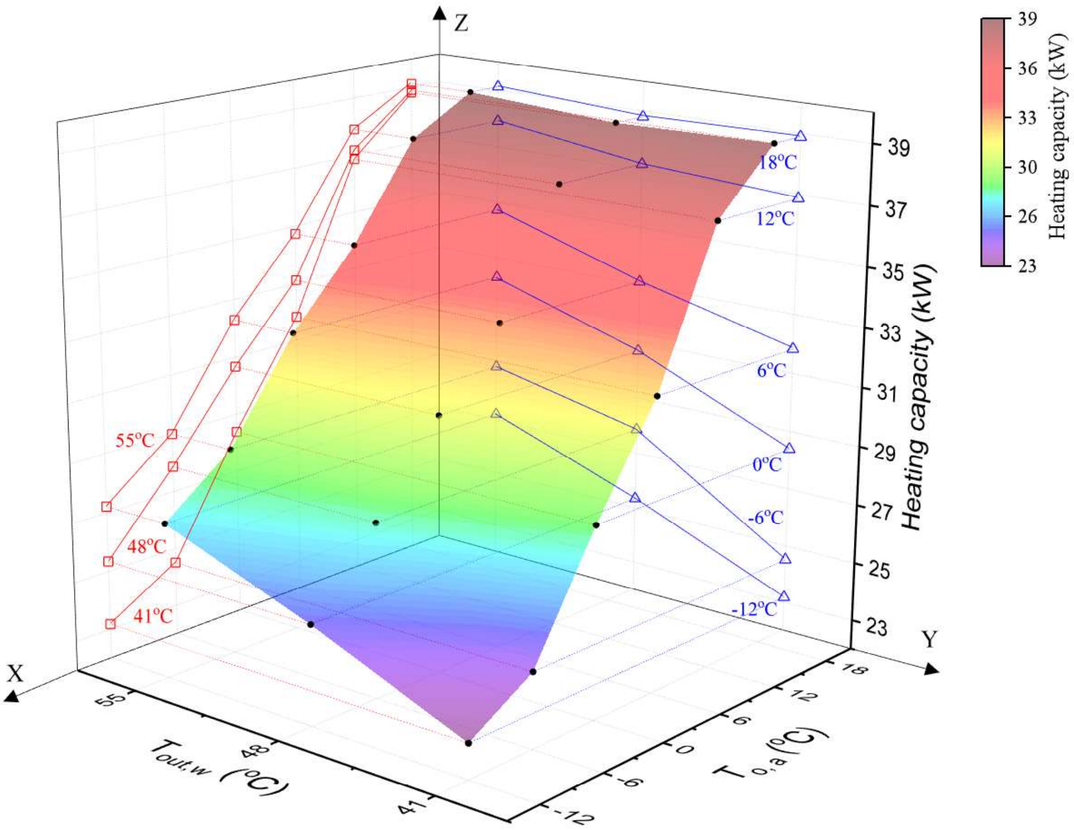

Figure 5. The heat capacity of THRHP under different working conditions

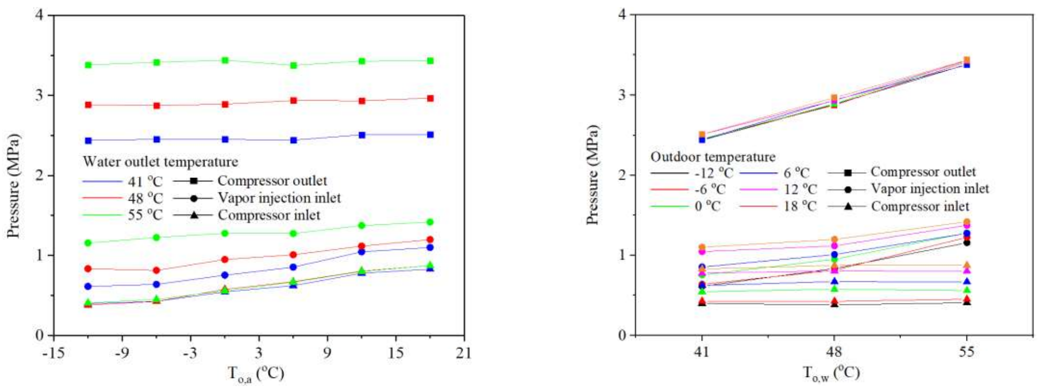

(a) (b)

Figure 6. The refrigerant pressures of THRHP under different working conditions (a) The influence of the outdoor temperature (b) The influence of the water outlet temperature

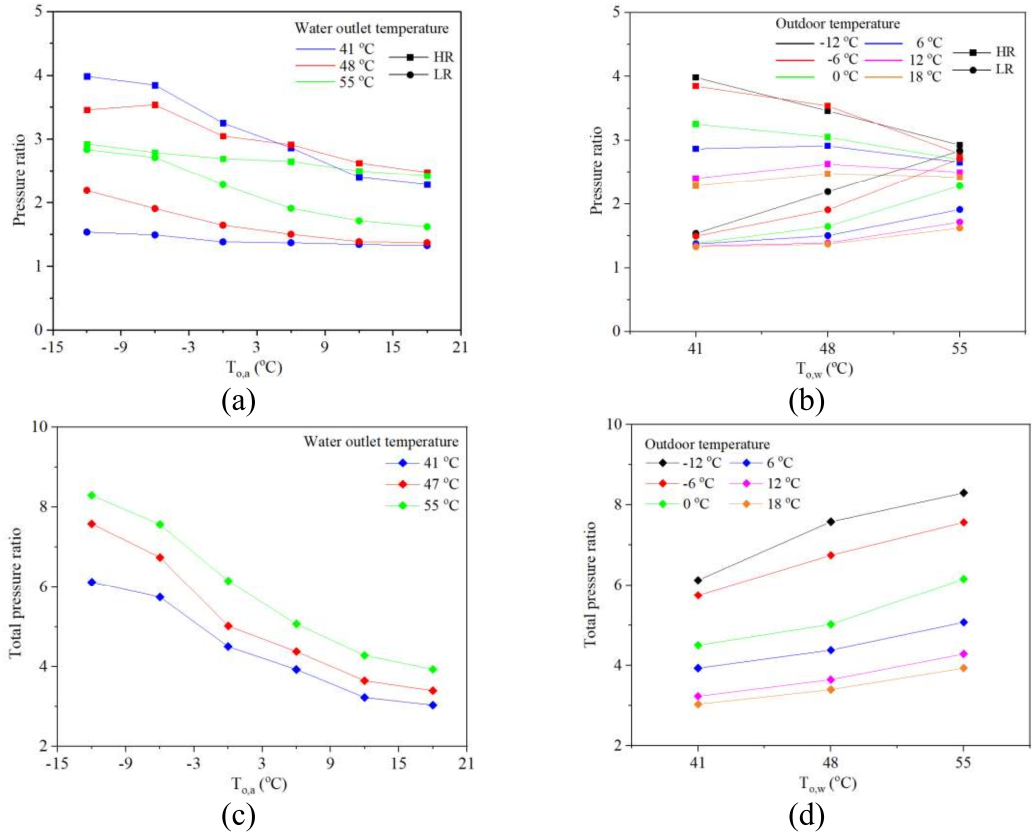

Figure 7. The Pressure ratios of THRHP under different working conditions (a) The influence of outdoor temperature on HR and LR (b) The influence of water outlet temperature on HR and LR (c) The influence of outdoor temperature on TR (d) The influence of water outlet temperature on TR

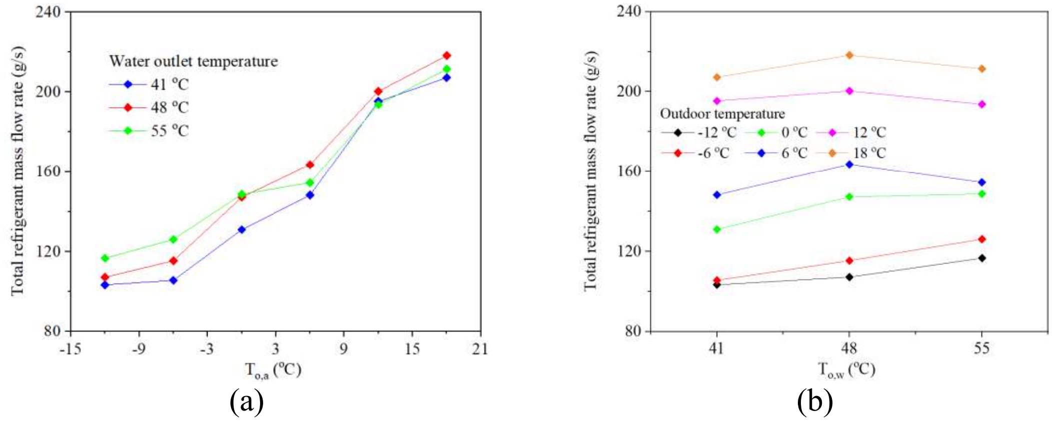

Figure 8. The total refrigerant mass flow rate under different working conditions (a) The influence of outdoor temperature (b) The influence of water outlet temperature

3.1.2 The impact on the power consumption of THRHP

Figure 9 shows the THRHP's power consumption characteristics under different working conditions (see the black spots). The X-Z projection shows the influence of the outdoor temperature (see the red spots), and the Y-Z projection shows the influence of the water outlet temperature (see the blue spots).

Respecting the influence of the outdoor temperature (see the X-Z projection of Figure 9), the variation from -12 ºC to 18 ºC has little effect on the THRHP's power consumption, whose maximum difference is 2.3%. The stable power consumption results from the effect of the refrigerant pressure variations. For instance, under the water outlet temperature of 41 ºC, Figure 6 (a) illustrates that the pressure of vapor injection inlet and compressor inlet increase by 108.1% and 79.5% with the outdoor temperature, respectively, and as a result of Figure 7 (a), the HR and LR decrease with outdoor temperature by 42.6% and 13.8%, respectively. According to Togashi et al [26] investigations, equation (9) indicates that the drops of LR along with the rises of refrigerant pressure of compressor inlet under the fixed refrigerant volumetric flow rate will keep the constant of low-pressure compression head (H_L), so as to the high-pressure compression head (H_H) according to equation (10). Therefore, according to equation (11), the variation of the power consumption of THRHP is stable with outdoor temperature, which is also consistent with the results of relevant papers [27-29].

$$H_L = \frac{k}{k-1} P_{r,\,in,\,com}\, v_L \left(LR^{\frac{k-1}{k}} - 1 \right) \tag{9}$$

$$H_H = \frac{k}{k-1} P_{r,\,com,\,inj}\, v_H \left(HR^{\frac{k-1}{k}} - 1 \right) \tag{10}$$

$$\left(H_L + H_H \right) = \eta W_{com} \tag{11}$$

where H_L and H_H are the compression head of low-pressure compression and high-pressure compression, respectively; W_{com} is the power consumption of the compressor; η is the compression efficiency of vapor injection compressor; k is the specific heat ratio; v is refrigerant volumetric flow rate.

In contrast, the water outlet temperature has a strong influence on the THRHP's power consumption (see the Y-Z projection of Figure 9), i.e., increasing the water outlet temperature from 41 ºC to 55 ºC raises the power consumption by around 34.0%. As Figure 6 (b) and Figure 7 (b) depicted, a higher water outlet temperature has little effect on the compressor inlet pressure but increases the LR. Thus, according to equation (9), the H_L increases with water outlet temperature. As for the H_H, according to equation (10), the decreasing HR and increasing vapor injection pressure jointly make the H_H stable. Finally, the total compression head of the vapor injection compressor rises with the water outlet temperature because of the increasing H_L, leading to the increasing power consumption of THRHP.

As result of the 3D surface of the power consumption in Figure 9, the power consumption surface rises rapidly as the water temperature increases, which is nearly perpendicular to the Y-Z plane. The maximum and minimum power consumption are 12.6 kW and 9.2 kW at -6 ºC /55 ºC and -12 ºC /41 ºC, respectively. Therefore, the water outlet temperature of the THRHP can be controlled to a lower value depending on the heating demand of the building, thus reducing energy consumption and achieving significant energy savings.

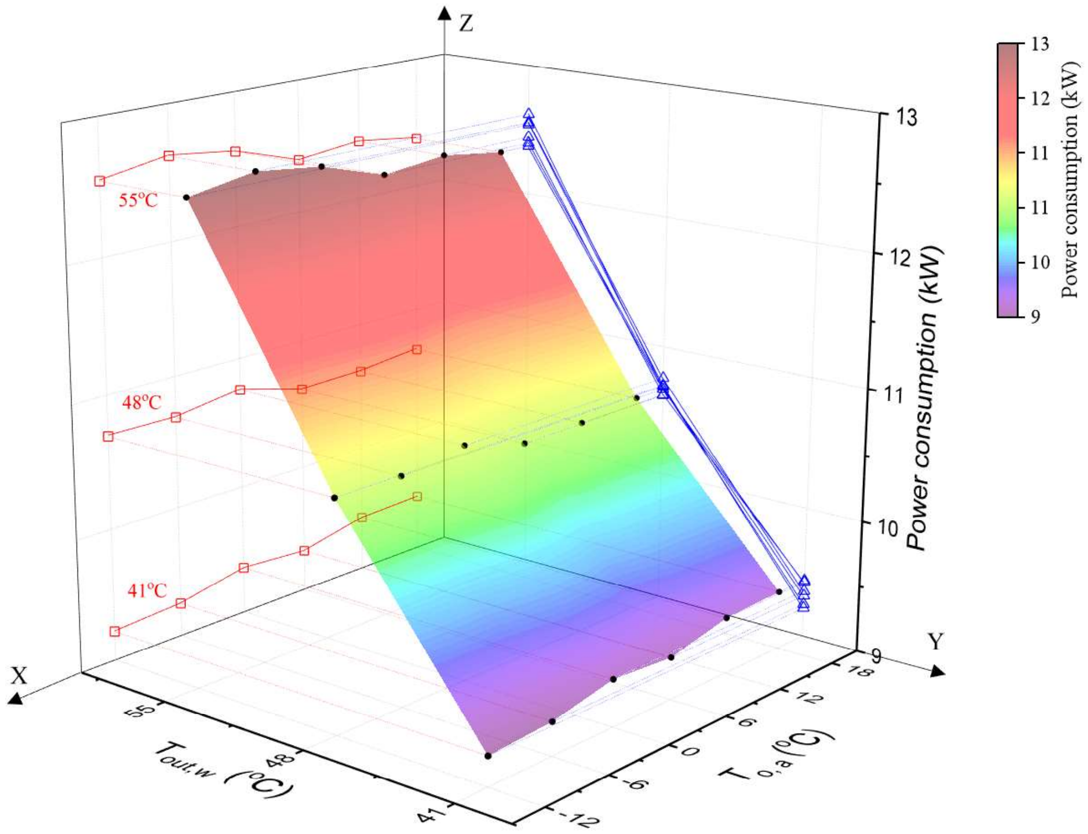

Figure 9. The power consumption of THRHP under different working conditions

3.1.3 The impact on the COP of THRHP

The COP of THRHP as a result of the interaction between the heating capacity and power consumption is given in Figure 10 (see the black spots), where the influence of the outdoor temperature is depicted by the X-Z projection (see the red spots), and the influence of the water outlet temperature is depicted by the Y-Z projection (see the blue spots).

Regarding the impact of outdoor temperature (see the X-Z projection of Figure 10), the COP of THRHP increases significantly when the outdoor temperature rises from -12 ºC to 18 ºC because of the sharp raising of the heat capacity and the stability of the power consumption as analyzed above, where it increases 64.0%, 53.5% and 45.8% at the water outlet temperature of 41 ºC, 48 ºC, 55 ºC, respectively.

Respecting the water outlet temperature increasing from 41 ºC to 55 ºC (see the Y-Z projection of Figure 10), a higher water outlet temperature reduces the COP because of the dramatically increasing power consumption. The COP drops by 23.3% at the outdoor temperature of 18 ºC. However, the drop in COP is less severe (16.5%) at outdoor temperatures of -12 ºC, because the increase in heating capacity is relatively significant at low outdoor temperatures as discussed above.

From the 3D surface of the COP in Figure 10, it can be seen that the COP decreases as the ambient temperature decreases and the water outlet temperature increases, falling in the shape of a ripple from the highest point. The THRHP reaches the maximum COP of 4.12 at 18 ºC/41 ºC, and drops to the minimum of 2.17 at -12 ºC/55 ºC, which is 52.7% of the maximum COP. More importantly, based on the 3D surface, it is found that to achieve the best seasonal average efficiency, the THRHP should decrease the water outlet temperature as the outdoor temperature rises after the satisfaction of building heating demand.

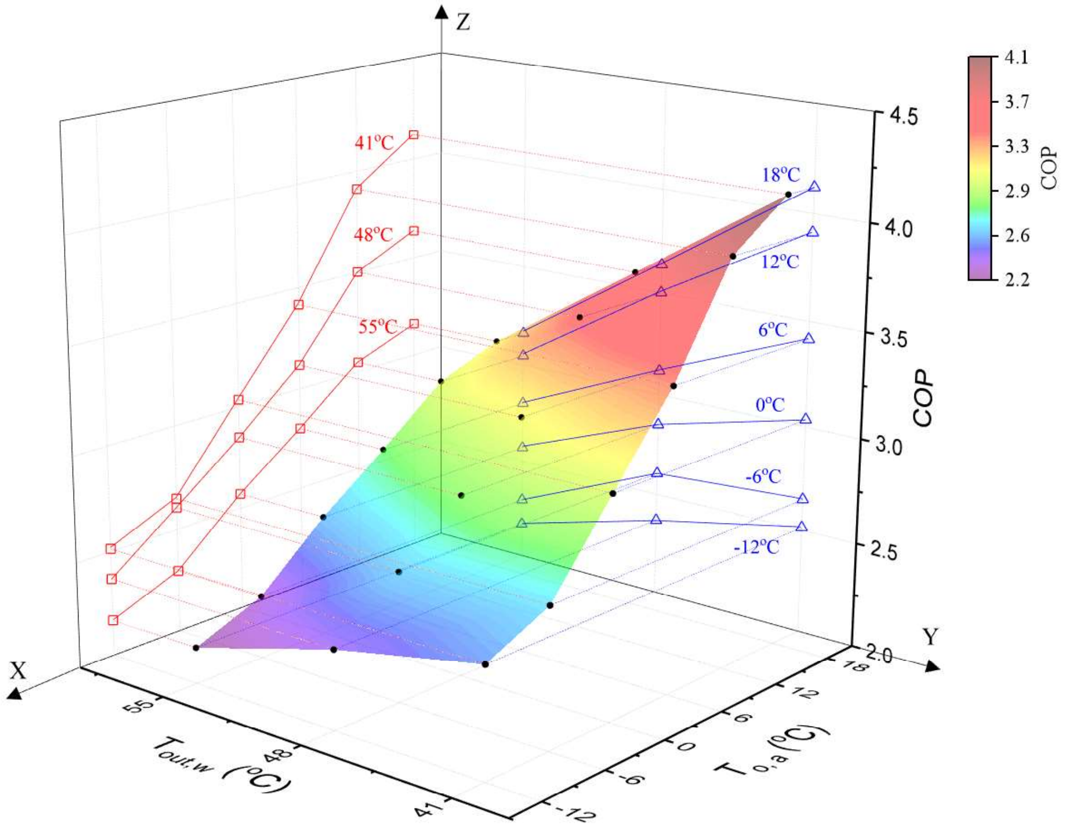

Figure 10. The COP of THRHP under different working conditions

3.1.4 The EVL opening adjustment for THRHP performance enhancement

Apart from the innovations of the THRHP geometry and process design, the EVL opening adjustment is key to achieving high performance of THRHP in cold climates. Figure 11 shows the optimum EVL openings found in the performance test (see the black spots).

From the X-Z projection of Figure 11, as a result of the influence of the outdoor temperature (see the red spots), the EVL opening should increase with the rise of outdoor temperature for a higher COP. Because as the outdoor temperature rises, increasing EVL opening raises the evaporation pressure and total refrigerant mass flow rate, therefore increasing heating capacity with stable power consumption, achieving higher COP. Furthermore, increasing EVL opening protects compressor inlet temperature from large superheats, ensuring THRHP's safe operation.

In contrast, for the influence of the water outlet temperature (see the blue spots in the Y-Z projection of Figure 11), the higher water outlet temperature requires a smaller EVL opening. Because a smaller EVL opening offers a stronger throttling effect on low-pressure evaporation to maintain the evaporation pressure when condensation pressure increases with the water outlet temperature. The evaporation pressure is stable to avoid too significant increases in power consumption. In addition, the small variation of evaporation pressure keeps the total refrigerant mass flow rate and evaporation temperature difference relatively stable with water outlet temperature, preventing liquid compression of THRHP.

The adjustment of EVL opening is critical to the optimum COP and safety of THRHP, which are beneficial to the studies on heat pump control strategies. On the basis of the optimized results, equation (12) of EVL opening is obtained by multivariate linear regression, and these optimized results in the 3D colour surface of EVL opening are programmed into the self-control scheme of THRHP for the best COP under different working conditions.

$$\theta_{\mathrm{EVL}} = 133.556 + 0.0245{T_{\mathrm{a,o}}}^2 + 0.034{T_{\mathrm{w,out}}}^2 - 0.0585T_{\mathrm{a,o}}T_{\mathrm{w,out}} + 3.8169T_{\mathrm{a,o}} - 3.9946T_{\mathrm{w,out}} \quad (12)$$

where θ_{EVL} is EVL opening in %, $T_{\mathrm{a,o}}$ is the outdoor temperature, $T_{\mathrm{w,out}}$ is the water outlet temperature. The coefficient of determination (R^2) of equation (12) of EVL opening is 0.95.

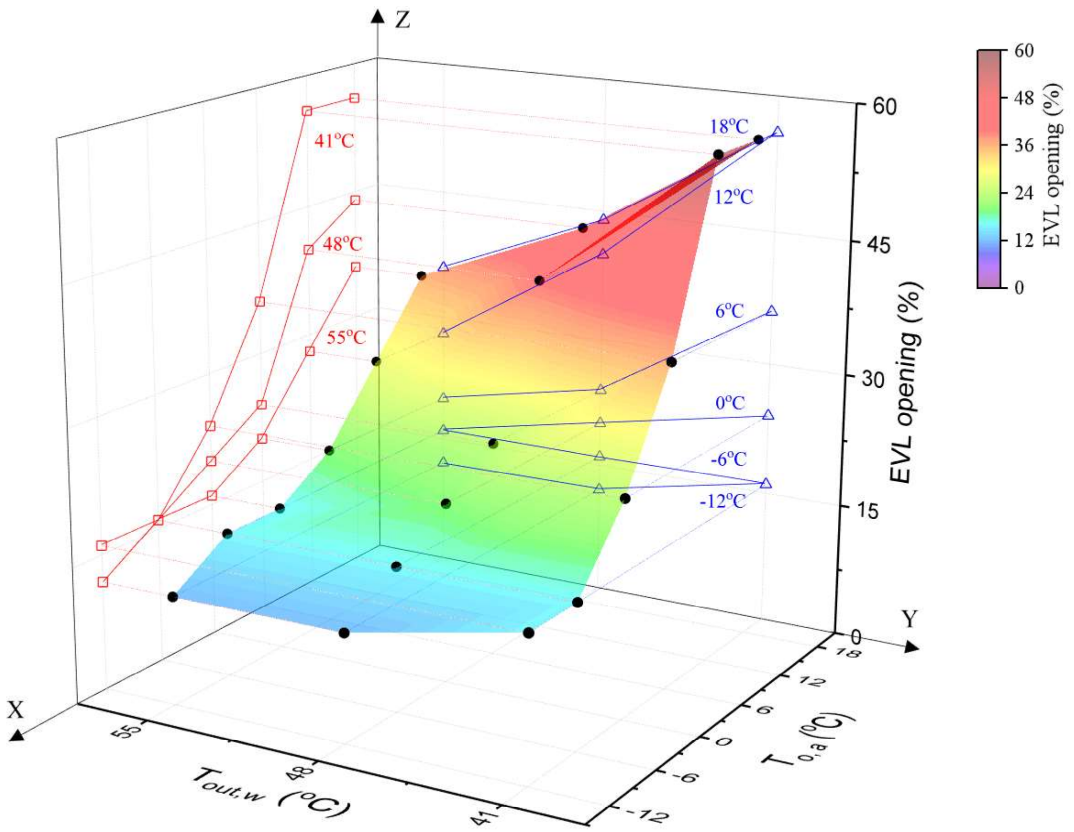

Figure 11. The optimum EVL opening for THRHP high performance

3.2 Impact of exhaust air heat recovery on the THRHP performance

In this section, the optimum performances of THRHP with and without exhaust air are compared and analyzed at outdoor/water outlet temperatures of -12 ºC/41ºC, -12 ºC/55 ºC and 18 ºC/55 ºC. For simplicity, the system without the exhaust air is called System-A, the system with exhaust air is called System-B, and the following working conditions of systems are continually named by outdoor temperature/water outlet temperature.

In Figure 12, the impacts of the exhaust air on the air temperature distribution of different systems are illustrated. The air temperatures at the exhaust air inlet of System-B are 34.2 ºC, 35.6 ºC, and 4.7 ºC higher than that of System-A under conditions of -12 ºC/41ºC, -12 ºC/55 ºC and 18 ºC/55 ºC, respectively. After the exhaust air of System-B mixes with the outdoor air, the air temperatures at the LE inlet are 10.1 ºC, 11.5 ºC and 0.9 ºC higher than that of System-A under conditions of -12 ºC/41ºC, -12 ºC/55 ºC and 18 ºC/55 ºC, respectively, which are notably narrowed because of the mixing of the main cold airflow from the outdoor air inlet.

In addition, respecting the temperature difference between the LE air inlet and the discharge air outlet, the temperature differences of System-B are larger than that of System-A under the three working conditions, which infers that the LE air flow rate of

System-B is smaller than that of System-A. According to the systems' design, System-B with the exhaust air cover and long exhaust air duct has a much higher airflow resistance when compared to System-A, and thus, System-B has a smaller air flow rate at the exhaust air inlet though it has additional exhaust air fans working. Further, after mixing with the outdoor air, the air flow rate at the LE air inlet of System-B remains smaller than that of System-A, and this decrease is also narrowed due to the mixing of the main cold airflow from the outdoor air inlet.

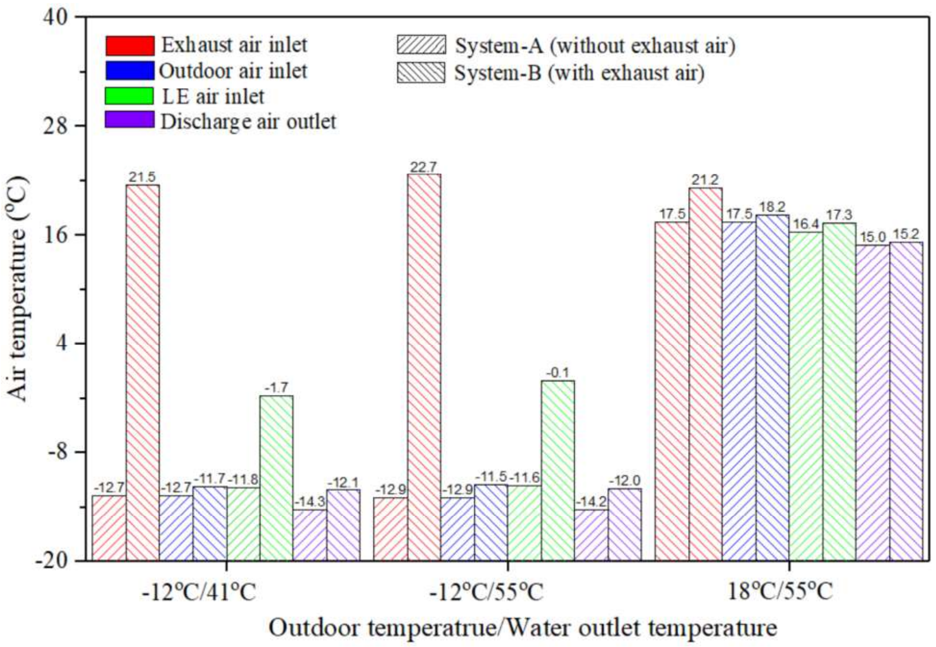

Figure 12. The air temperature of systems with/without exhaust air

3.2.1 The heating capacity of systems with/without exhaust air

From Figure 13, it is shown that the impacts of exhaust air on heat capacity are different under three working conditions. Under the working conditions of -12 ºC/41ºC, the heating capacity of System-B has a slight improvement of 2.7% compared to System-A. According to the results in Figure 12, the higher exhaust air inlet temperature of System-B has a positive impact while the smaller exhaust air flow rate has a negative impact on the vapor injection pressure. Under the integrated impact, the vapor injection pressure of System-B decreases by 0.3% compared to System-A (see Figure 14 (a)), which will lead to a smaller refrigerant mass flow rate. Regarding the compressor inlet, the integrated impact of the higher LE's air temperature and smaller LE's air flow rate eventually leads to the 8.5% increase in the compressor inlet pressure of System-B when compared to System-A (see Figure 14 (b)), which will increase the refrigerant mass flow rate. Combining the results of vapor injection inlet and compressor inlet, the total refrigerant mass flow rate of System-B is increased, contributing to the improvement of heating capacity.

When the working condition changes to -12 ºC/55 ºC, the vapor injection pressure level rises a lot as the water temperature increases from 41 ºC to 55 ºC. Under these conditions, the negative impact of the smaller exhaust air flow rate is overwhelmed and the dominant positive impact of the higher exhaust air temperature causes the increase in vapor injection pressure of System-B by 15.8% compared to System-A (see Figure 14 (a)). Respecting the compressor inlet pressure, the higher LE's air inlet temperature causes the increase in compressor inlet pressure of System-B by 6.1% when compared to System-A (see Figure 14 (b)). As a result of the increasing vapor injection pressure and increasing compressor inlet pressure, the total refrigerant mass flow rate increases obviously, so as to the 26.9% improvement in the heating capacity of System-B when compared to System-A.

Regarding the working conditions of 18 ºC/55 ºC, the outdoor air temperature is close to the exhaust air temperature, and the LE air inlet temperature increase of System-B is small. As a result, under the equivalent impacts from the increased air temperature and the decreased air flow rate at the exhaust air inlet, the vapor injection pressure of System-B is 0.7% higher than that of System-A (see Figure 14 (a)). When it comes to the compressor inlet, the negative impact of the smaller air flow rate of System-B results in a 3.8% decrease in compressor inlet pressure since the LE air inlet temperature of System-B is only 0.9 ºC higher than that of System-A (see Figure 14 (b)). Eventually, the decreased compressor inlet pressure reduces the total refrigerant mass flow rate and thus causing a 4.4% decline in the heating capacity of System-B compared to System-A.

From the results of heating capacity comparisons, the high-temperature exhaust air can effectively improve the heating capacity under the conditions of low outdoor temperature, i.e., -12 ºC/41ºC and -12 ºC/55 ºC, but the additional accessories, i.e., the exhaust air cover and long exhaust air duct, which lead to the smaller air flow rate will overwhelm the little temperature increase of exhaust air, and eventually cause the reduction of heating capacity under the conditions of high outdoor temperature, i.e., 18 ºC/55 ºC.

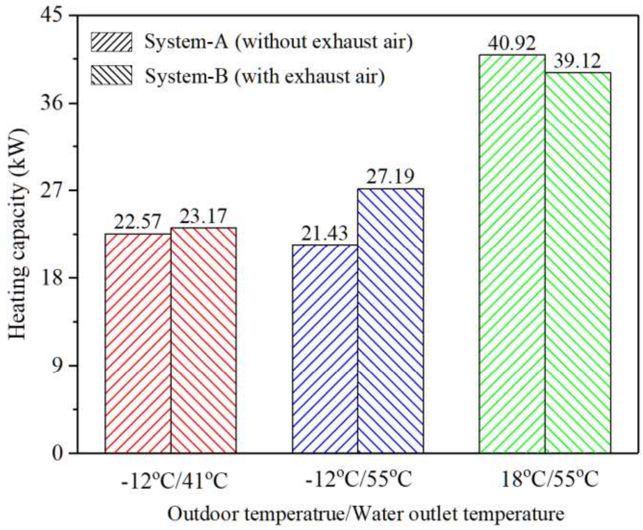

Figure 13. The heating capacity of systems with/without exhaust air

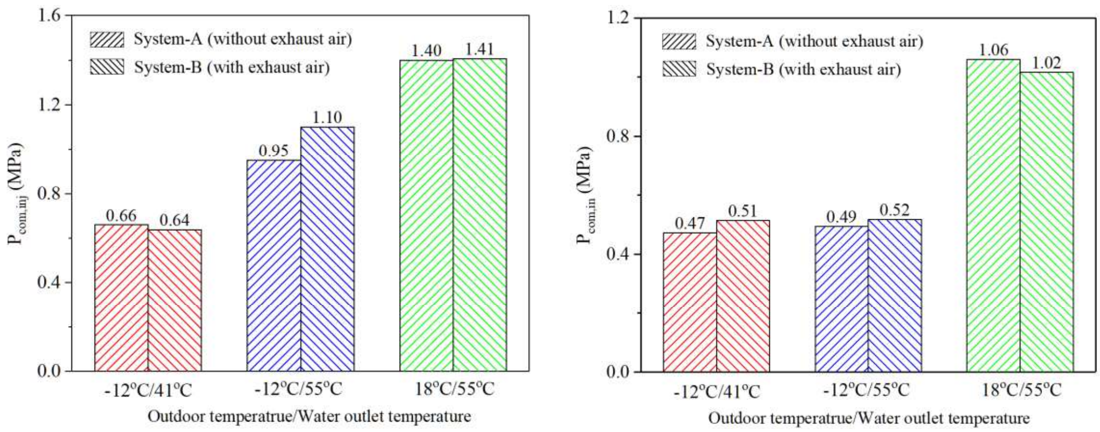

(a) (b)

Figure 14. The refrigerant pressure of systems with/without exhaust air (a) vapor injection pressure (b) compressor inlet pressure

3.2.2 The power consumption of systems with/without exhaust air

Figure 15 illustrates the power consumption difference between System-A and System-B at -12 ºC/41ºC, where the power consumption of System-B is 0.4% higher than that of System-A. The impact of the decreased vapor injection pressure counteracts the impact of the increased compressor inlet pressure (see Figure 14), combined with the additional power consumption of the exhaust air fans, eventually leading to the small rise in the power consumption of System-B.

In terms of the variation at -12 ºC/55 ºC, the power consumption of System-B is 5.1% higher than that of System-A. As discussed above, the vapor injection pressure of System-B increases a lot under this high water outlet temperature condition when compared to System-A, leading to the more obvious rise in total refrigerant mass flow rate and thus the power consumption of System-B.

Concerning those at 18 ºC/55 ºC, the integrated impact of the vapor injection pressure and compressor inlet pressure decreases the total refrigerant mass flow rate. However, additional exhaust air fans eventually result in the ascent in the power consumption of System-B by 2.3% compared to System-A.

From the results of the power consumption comparison, the high-temperature exhaust air and additional exhaust air fans will cause 0.4% to 5.1% increases in the power consumption of the system with exhaust air heat recovery, which is relatively small under the low outdoor temperature conditions. It can be inferred that the exhaust air heat recovery has a less negative impact on system efficiency as the outdoor temperature declines, being more advantageous at low outdoor temperature conditions.

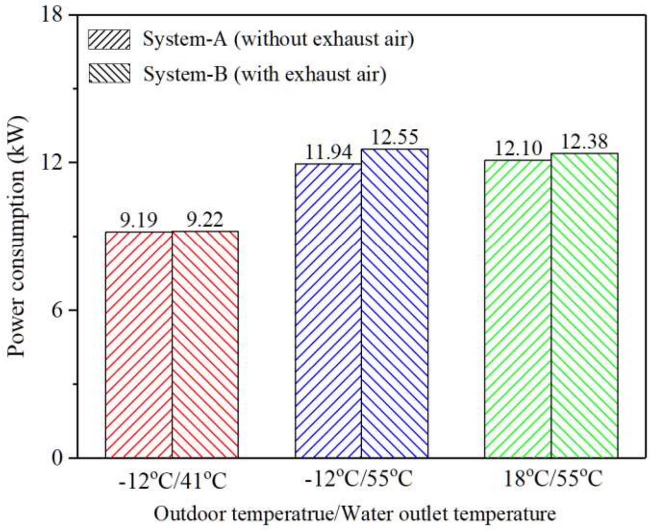

Figure 15. The power consumption of systems with/without exhaust air

3.2.3 The COP of systems with/without exhaust air

The variations of COP in Figure 16 are highly relevant to the heating capacity and power consumption of the systems. Under the conditions of -12 ºC/41 ºC, System-B achieves a 2.7% improvement in the heating capacity from the higher exhaust air temperature, while its power consumption is basically unchanged, thereby, the COP of System-B is 2.0% higher than that of System-A.

When the water outlet temperature increases to 55 ºC, i.e., under the conditions of -12 ºC/55 ºC, due to the significant increase in the vapor injection pressure of System-B by 15.8% (see Figure 14), the heating capacity and power consumption of System-B are increased by a relatively large amount, 26.9% and 5.1% respectively. Eventually, the increase of COP of System-B reaches 21.2% due to the significant increase in the heating capacity.

However, when the outdoor temperature rises to 18 ºC, i.e, under the conditions of 18

°C/55 °C, the heating capacity of System-B decreases by 4.4% because of the small improvement of the exhaust air temperature when compared to System-A. Combined with the 2.3% rise in the power consumption of System-B, the COP of System-B is 6.5% lower than that of System-A.

To sum up the performance comparison of systems with and without exhaust air, the positive effects of exhaust air on the heating capacity and COP can be fully brought into play under the conditions of low outdoor temperature and high water outlet temperature, which are the most common in the practical application of heat pumps. However, under high outdoor temperature conditions, exhaust air heat recovery weakens the heating capacity and COP. Therefore, the exhaust air fans should be turned off when the outdoor temperature exceeds 18 °C, and more researches need to be conducted to investigate a better control method for the exhaust air flow rate.

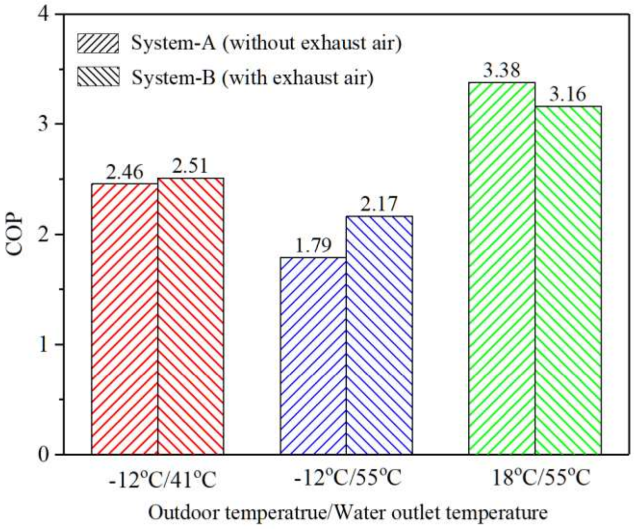

Figure 16. The COP of systems with/without exhaust air

3.2.4 The defrosting performance with exhaust air

Besides heating performance, the defrosting performances of THRHP under different working conditions are also measured as shown in Figure 17. The THRHP defrost program is set to start when the compressor inlet temperature is detected to be below 3 °C, at which point the THRHP will defrost for 4 minutes every 20 minutes of heating operation. During defrost, the compressor will stop working and only the exhaust air fans will extract the indoor exhaust air to defrost the heat pump's outdoor heat exchanger surface to ensure that it is not covered in ice. After each 4-minute defrost, the THRHP compressor will start again to produce heat.

As the results are shown in Figure 17 (a), under the conditions of -6 °C/41 °C, the heating capacity and COP of THRHP have an obvious deterioration during the 20 minutes heating operation, which means increasing frost. The defrosting starts after the 20 minutes of heating operation, which only consumes 0.46 kW. According to the results of the next heating operation circuit, it can be seen that after the 4 minutes of exhaust air defrosting, the degradations in heating capacity and COP are eliminated and returns to the initial level again in the next heating operation cycle.

Under the conditions of 0 ºC/41 ºC (see Figure 17 (b)), the heating capacity and COP of THRHP are less deteriorated during the 20 minutes heating operation, indicating that the level of frost diminished as the outdoor temperature increased. However, the exhaust air defrosting process is performed according to the program, which takes only 4 minutes and consumes only 0.46 kW, and effectively guarantees a good performance in every heating operation cycle.

From the results of the defrosting experiments, it is clear that the exhaust air defrosting method designed for the THRHP can effectively remove frost (4 minutes) from the outdoor heat exchanger with very low power consumption (0.46 kW) under various working conditions, ensuring the stable and efficient heating performance of THRHP.

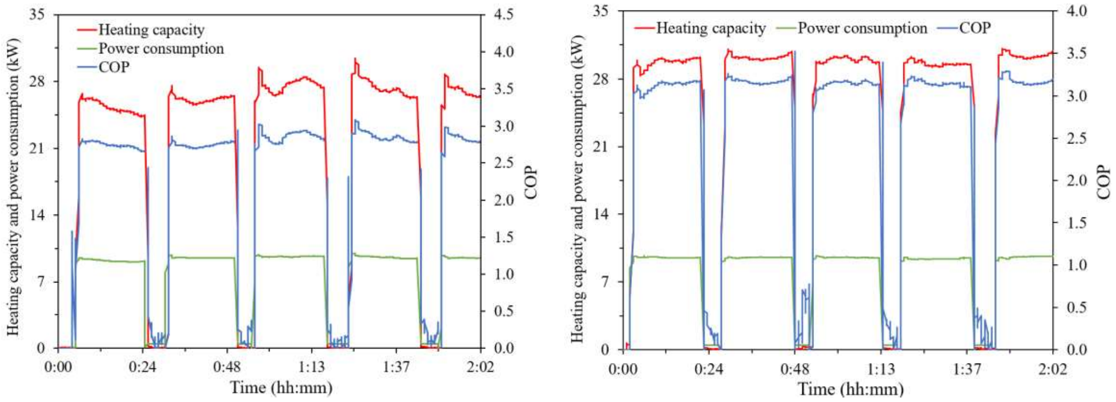

(a) (b)

Figure 17. Defrosting performance of THRH under (a) the conditions of -6 ºC /41 ºC (b) the condition of 0 ºC /41 ºC

3.3 Performance comparison of THRHP and commercial heat pumps

Performance comparisons with commercial heat pumps are illustrated in Figure 18 to Figure 20. The collected commercial heat pumps are air-to-water heat pumps without any heat recovery component, whose heating performance data is collected from their official materials. Performance details of the heat pumps are compared under a wide range of outdoor temperatures between -12 ºC and 7 ºC. It is worth noting that the high water outlet temperature is crucial for wider heat pump deployment because most existing houses are equipped with radiators along with gas boilers, which require high-temperature water to achieve space heating. High-water-temperature heat pumps can replace the gas boiler directly without a high initial cost for retrofitting, thus accelerating the deployment of heat pumps. In addition, the high water temperature has an antibacterial effect to improve the safety of the heat pump system. So, the comparisons are conducted under a high water outlet temperature of 55 ºC.

3.3.1 Comparison of heating capacity with commercial heat pumps

The heating capacity is variable in different models and brands and is dependent on the size of heat pumps, e.g., the heat exchanger area and compressor discharge volume. Therefore, the absolute values of heating capacity are not comparable. However, the stability of heating capacity when outdoor temperature decreases is an important factor in guaranteeing the user's thermal comfort. Figure 18 shows that the heating capacity of THRHP maintains a 78.4% heating capacity when outdoor temperature decreases from 6 ºC to -12 ºC. Regarding commercial heat pumps, the model of 30AWH004H can only maintain 59.5% heating capacity, while the model of 30AWH006H maintains 60.7%, and the model of 30AWH012H maintains 62.0% when outdoor temperature decreases from 7 ºC to -7 ºC. The comparison results indicate that benefiting from the exhaust air which increases the evaporation temperature of THRHP and thus guarantees its heating capacity when the outdoor temperature decreases, THRHP offers stronger stability of heating capacity than the commercial heat pumps.

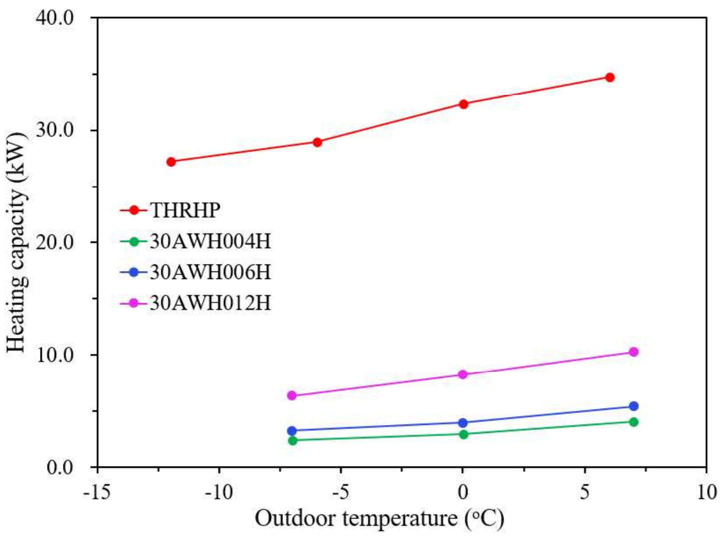

Figure 18. The heating capacity of heat pumps under different outdoor temperatures

3.3.2 Comparison of power consumption with commercial heat pumps

The absolute values of power consumption of different brands of heat pumps mainly depend on the size of compressors, which are not comparable. But Figure 19 depicts that the power consumption of THRHP remains steady (only a 2.0% increase) when the outdoor temperature raises from -12 ºC to 6 ºC, whereas the power consumptions of the commercial heat pumps increase a lot as the outdoor temperature rises from -7 ºC to 7 ºC. For instance, the power consumption of 30AWH004H, 30AWH008H and 30AWH012H increased by 10.4%, 21.2% and 16.1%, respectively. Thus, the power consumption of THRHP has less effect by outdoor temperature, so as to save energy bills for the users.

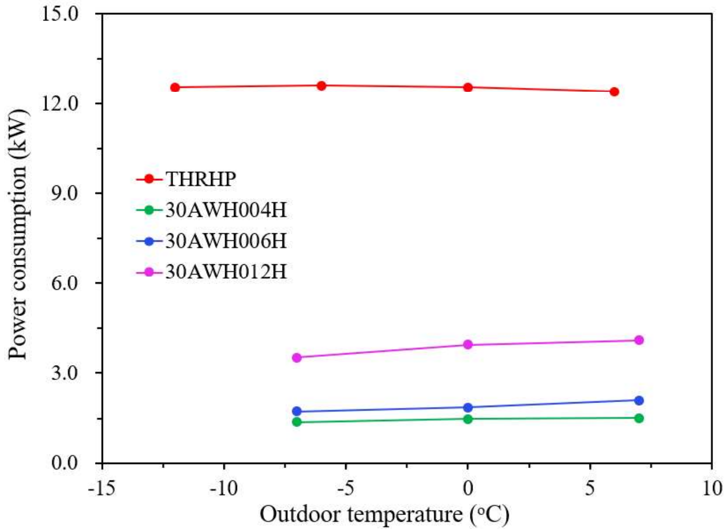

Figure 19. The power consumption of heat pumps under different outdoor temperatures

3.3.3 Comparison of COP with commercial heat pumps

Figure 20 shows that the COPs of the commercial heat pumps are not higher than 2.12 at the outdoor temperature of -7 ºC, whilst that of THRHP has achieved 2.17 at even -12 ºC and increases to 2.30 at -6 ºC. Furthermore, at the same outdoor temperature of 0 ºC, the highest COP of commercial heat pumps is 2.14, i.e., the model 30AWH006H, whereas the COP of THRHP is 2.57, which is 20.1% higher. The comparisons of COP under low outdoor temperature conditions illustrate that the THRHP performs much better than normal heat pumps because of the benefits of the innovative designs of exhaust air heat recovery.

When it comes to performance under high outdoor temperature conditions, the COP of the 30AWH004H is 2.71 at the outdoor temperature of 7 ºC, while that of THRHP is 2.8 at the outdoor temperature of 6 ºC, which only has a 1.5% difference. It is found that the improvement benefited from the exhaust air heat recovery of THRHP is reduced under the higher outdoor temperature conditions when compared to the commercial normal heat pumps, which is consistent with the results obtained earlier.

Additionally, owing to the good stability of heating capacity and power consumption, THRHP has more stable COP, which decreases by 22.6% as outdoor temperature decreases from 6 ºC to -12 ºC, while that of 30AWH006H, 30AWH006H, and 30AWH012H respectively reduce by 34.3%, 26.4%, and 28.0% when the outdoor temperature only decreases from 7 ºC to -7 ºC. A detailed comparison with more commercial heat pumps, as listed in Table 6, further shows that the novel THRHP has a higher COP than the normal commercial heat pumps in the range of the operating conditions.

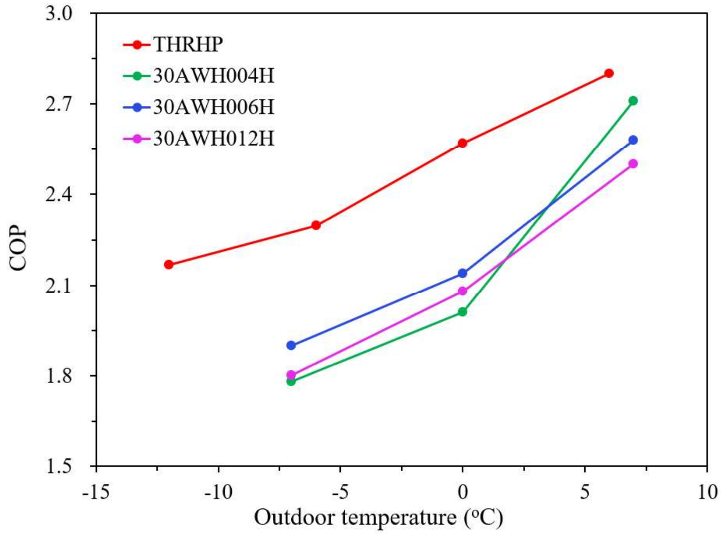

781

782 Figure 20. The COP of heat pumps under different outdoor temperatures

Table 6. Performance comparison with commercial heat pumps

Brand	Model number	Testing conditions		Heating performance			Refrigerant
		Outdoor temperature (°C)	Water outlet temperature (°C)	Heating capacity (kW)	Power consumption (kW)	COP	
Panasonic	KIT-AXC09HE5	-7	55	9.00	4.46	2.02	R410a
	KIT-AXC12HE5	-7	55	12.00	6.25	1.92	R410a
	KIT-ADC09JE5-1	-7	55	5.90	3.06	1.93	R32
	WH-MXC09J3E5	-7	55	9.00	4.25	2.12	R32
	WH-MXC12J6E5	-7	55	12.00	6.00	2.00	R32
	WH-MDC09J3E5	-7	55	7.00	3.89	1.80	R32
Carrier	30AWH004H	-7	55	2.44	1.37	1.78	R410a
	30AWH006H	-7	55	3.28	1.73	1.90	R410a
	30AWH012H	-7	55	6.37	3.54	1.80	R410a
Calorex	PRO-PAC30H	0	55	11.60	6.00	1.93	R134a
	PRO-PAC45H	0	55	14.40	7.60	1.89	R134a
	PRO-PAC70H	0	55	21.70	10.90	1.99	R134a
	PRO-PAC90H	0	55	28.80	15.20	1.89	R134a
	PRO-PAC140H	0	55	43.40	21.80	1.99	R134a
Carrier	30AWH004H	0	55	2.99	1.49	2.01	R410a
	30AWH006H	0	55	3.97	1.86	2.14	R410a
	30AWH012H	0	55	8.23	3.96	2.08	R410a
Midea	MHC-V5W/D2N8	7	55	4.65	1.77	2.63	R32
	MHC-V9W/D2N8	7	55	8.60	3.13	2.75	R32
	MHC-V16W/D2N8	7	55	16.10	5.91	2.72	R32
	MHC-V16W/D2RN8	7	55	16.10	5.83	2.76	R32
LG	HM051M.U43	7	55	5.50	2.04	2.70	R32
	HM071M.U43	7	55	5.50	2.04	2.70	R32
	HM091M.U43	7	55	5.50	2.04	2.70	R32
Carrier	30AWH004H	7	55	4.10	1.51	2.71	R410a
	30AWH006H	7	55	5.40	2.09	2.58	R410a
	30AWH012H	7	55	10.27	4.11	2.50	R410a
University of Hull	THRHP	-12	55	27.22	12.55	2.17	R410a
	THRHP	-6	55	28.99	12.62	2.30	R410a
	THRHP	0	55	32.29	12.56	2.57	R410a
	THRHP	6	55	34.73	12.40	2.80	R410a
	THRHP	12	55	37.91	12.45	3.05	R410a
	THRHP	18	55	39.12	12.38	3.16	R410a

3.4 Future works

Although the THRHP increases the heating capacity by using exhaust air heat recovery, it may decrease the system performance in warm weather. Therefore, it is critical to apply a self-control scheme to adjust the exhaust air heat recovery and expansion valve opening to achieve the best seasonal heating performance in real-life applications. The THRHP is going to be installed at Hull Central Library, UK, to provide space heating for a working room. The long-term test will be ongoing with many sensors installed for monitoring system performance and stability. The future work will focus on THRHP's long-term operation and economic and environmental performance.

4 **Conclusion**

A novel two-stage heat recovery heat pump (THRHP) is proposed and manufactured in this study to overcome the low COP and high energy consumption barriers with the existing heat pump. The THRHP extracts heat from exhaust air and outdoor ambient to increase heating capacity and COP while reducing power consumption by using vapor injection compressor. Based on experiment optimization and analysis, more insights into the THRHP were obtained and the results show that the THRHP has excellent heating characteristics and performance, as follows.

(1) The characteristics analysis reveals that the heating capacity of THRHP declines as outdoor temperature decreases but can increase up to 17.5% with water outlet temperature, while the power consumption of THRHP is only sensitive to water outlet temperature, reducing by up to 26.7% with decreasing water outlet temperature. As a result, the COP of THRHP decreases with descending outdoor temperature but increases up to 64.0% with declining water outlet temperature. A system control strategy is suggested to achieve the best energy efficiency of THRHP in the application. The water outlet temperature should be increased when the outdoor temperature drops to ensure indoor temperature and thermal comfort, and reduced when the outdoor temperature rises to increase COP and save energy.

(2) Based on analysis of exhaust air's impact, the characteristics of THRHP are further revealed. At low outdoor temperature conditions, i.e., -12 ºC/41 ºC and -12 ºC/55 ºC of outdoor temperature/water outlet temperature, the heat recovery from exhaust air increases the heating capacity by 2.66% and 26.88%, leading to the COP increase by 2.03% and 21.23%, respectively. At conditions of high outdoor temperature, i.e., 18 ºC/55 ºC, the exhaust air has negative impacts, which not only decreases the heating capacity but also increases the power consumption, leading to a 6.51% decline in COP. Further, defrosting results show that the exhaust air gives a fast and efficient process to the THRHP, which has a defrosting power of 0.46 kW while the associated defrosting time is 4 mins.

(3) Compared to commercial heat pumps, the THRHP produces a more stable heating capacity and power consumption as outdoor temperature changes, which are essential features for meeting building heat loads and reducing energy consumption in cold climate applications. Under the low outdoor temperature and high water outlet temperature condition of 0 °C/55 °C, the THRHP achieves 20.1% higher COP than the commercial heat pump, making it highly competitive with market products.

(4) According to the optimization result of THRHP, the optimal expansion valve opening control and exhaust air fans situation are programmed into the THRHP for the best COP under various working conditions. Further, based on the characteristics of THRHP, the system control strategy is suggested for the best average efficiency in application. The novel THRHP with optimization strategies can significantly improve the performance of air source heat pumps and their competitiveness against traditional gas heating equipment, accelerating the deployment of low-carbon heating equipment and advancing the process of carbon neutrality.

Acknowledgement

This work is funded by the UK BEIS project 'A low carbon heating system for existing public buildings employing a highly innovative multiple-throughout-flowing micro-channel solar-panel-array and a novel mixed indoor/outdoor air source heat pump' (LCHTIF1010) and International Exchange 2021 Cost Share (IEC\NSFC\211237). This work is also sponsored by the Chinese Scholarship Council.

References

[1] Global energy transformation-a roadmap to 2050, International renewable energy agency, 2019.

[2] Renewables 2019-analysis and forecast to 2024, International energy agency, 2019.

[3] Heat pumps: more efforts needed, International energy agency, https://www.iea.org/reports/heat-pumps, 2021.

[4] Heat and Buildings Strategy, The Secretary of State for Business, Energy and Industrial Strategy, https://www.gov.uk/government/publications/heat-and-buildings-strategy, 2021.

[5] L. Yang, Heat pump market development in China, International energy agency, https://heatpumpingtechnologies.org/publications/heat-pump-market-development-in-china/, 2020.

[6] X. Chen, Y. Zhou, J. Yu, A theoretical study of an innovative ejector enhanced vapor compression heat pump cycle for water heating application, Energy Build. 43(12) (2011) 3331-3336.

[7] L. Zhu, J. Yu, M. Zhou, X. Wang, Performance analysis of a novel dual-nozzle ejector enhanced cycle for solar assisted air-source heat pump systems, Renew.

Energy 63 (2014) 735-740.

[8] D. Wang, Y. Liu, Z. Kou, L. Yao, Y. Lu, L. Tao, P. Xia, Energy and exergy analysis of an air-source heat pump water heater system using CO2/R170 mixture as an azeotropy refrigerant for sustainable development, International Journal of Refrigeration 106 (2019) 628-638.

[9] B. Xiao, H. Chang, L. He, S. Zhao, S. Shu, Annual performance analysis of an air source heat pump water heater using a new eco-friendly refrigerant mixture as an alternative to R134a, Renew. Energy 147 (2020) 2013-2023.

[10] B. Luo, Theoretical study of R32 in an oil flooded compression cycle with a scroll machine, International Journal of Refrigeration 70 (2016) 269-279.

[11] Z. Yuan, Q. Liu, B. Luo, Z. Li, J. Fu, J. Chen, Thermodynamic analysis of different oil flooded compression enhanced vapor injection cycles, Energy 154 (2018) 553-560.

[12] K. Takezato, S. Senba, T. Miyazaki, N. Takata, Y. Higashi, K. Thu, Heat Pump Cycle Using Refrigerant Mixtures of HFC32 and HFO1234yf, Heat Transfer Engineering 42(13-14) (2020) 1097-1106.

[13] S.S. Bertsch, E.A. Groll, Two-stage air-source heat pump for residential heating and cooling applications in northern U.S. climates, International Journal of Refrigeration 31(7) (2008) 1282-1292.

[14] V. Baxter, E. Groll, B. Shen, Air source heat pumps for cold climate applications, REHVA journal (2014) 14-18.

[15] X. Xu, Y. Hwang, R. Radermacher, Refrigerant injection for heat pumping/air conditioning systems: Literature review and challenges discussions, International Journal of Refrigeration 34(2) (2011) 402-415.

[16] B. Shen, O. Abdelaziz, V. Baxter, E. Vineyard, Cold Climate Heat Pump Using Tandem Vapor-Injection Compressors, Cold Climate HVAC 20182019, pp. 429-439.

[17] S. Lu, J. Zhang, R. Liang, J. Wang, Heating and power generation characteristics of the vapor injected photovoltaic-thermal heat pump system, Renew. Energy 192 (2022) 678-691.

[18] G.V. Fracastoro, M. Serraino, Energy analyses of buildings equipped with exhaust air heat pumps (EAHP), Energy Build. 42(8) (2010) 1283-1289.

[19] S.B. Riffat, M.C. Gillott, Performance of a novel mechanical ventilation heat recovery heat pump system, Appl. Therm. Eng. 22(7) (2002) 839-845.

[20] A. Nguyen, Y. Kim, Y. Shin, Experimental study of sensible heat recovery of heat pump during heating and ventilation, International Journal of Refrigeration 28(2) (2005) 242-252.

[21] M. Gustafsson, G. Dermentzis, J.A. Myhren, C. Bales, F. Ochs, S. Holmberg, W. Feist, Energy performance comparison of three innovative HVAC systems for renovation through dynamic simulation, Energy Build. 82 (2014) 512-519.

[22] F. Fucci, C. Perone, G. La Fianza, L. Brunetti, F. Giametta, P. Catalano, Study of a prototype of an advanced mechanical ventilation system with heat recovery integrated by heat pump, Energy Build. 133 (2016) 111-121.

[23] J. Pu, C. Shen, C. Zhang, X. Liu, A semi-experimental method for evaluating frosting performance of air source heat pumps, Renew. Energy 173 (2021) 913-925.
[24] M. Song, S. Deng, C. Dang, N. Mao, Z. Wang, Review on improvement for air source heat pump units during frosting and defrosting, Appl. Energy 211 (2018) 1150-1170.
[25] A. Ege, H.M. Şahin, Uncertainties in energy and exergy efficiency of a High Pressure Turbine in a thermal power plant, International Journal of Hydrogen Energy 41(17) (2016) 7197-7205.
[26] E. Togashi, M. Satoh, Development of variable refrigerant flow heat-pump model for annual-energy simulation, Journal of Building Performance Simulation 14(5) (2021) 554-585.
[27] D. Wu, J. Jiang, B. Hu, R.Z. Wang, Experimental investigation on the performance of a very high temperature heat pump with water refrigerant, Energy 190 (2020).
[28] X. Peng, J. Xie, X. Liu, G. Wang, D. Wang, Y. Yang, Experimental investigation and comparison on heating performance characteristics of two transcritical CO2 heat pump systems, Energy Build. 250 (2021).
[29] J. Chen, R. Ding, Y. Li, X. Lin, Y. Chen, X. Luo, Z. Yang, Application of a vapor–liquid separation heat exchanger to the air conditioning system at cooling and heating modes, International Journal of Refrigeration 100 (2019) 27-36.